Soil Dynamics and Earthquake Engineering 111 (2018) 53–64

Contents lists available at ScienceDirect

Soil Dynamics and Earthquake Engineering

journal homepage: www.elsevier.com/locate/soildyn

Seismic bearing capacity of surficial foundations on sloping cohesive ground

Ozer Cinicioglu*, Anil Erkli

Dept. of Civil Engineering, Bogazici University, Istanbul, Turkey

ARTICLE INFO

Keywords:
Seismic bearing capacity
Slopes
Finite element method
Shallow foundation
Cohesive soil

ABSTRACT

Engineers often assume undrained conditions in stability calculations of shallow foundations resting on soil with fine content as this assumption yields conservative results. Calculation of undrained bearing capacity of shallow foundations on level ground is a well-defined problem and when the footing is located on or near slopes, empirical equations or design charts produced based on limit equilibrium, upper bound plasticity calculations or finite element method (FEM) analyses are used. On the other hand, available studies that consider seismic bearing capacity of foundations on cohesive soils do not consider the influences of all influential parameters. Therefore, their use in design practice is rather limited. Accordingly, this study attempts to develop design charts that consider the influences of all parameters that affect the undrained bearing capacity factor of surficial strip footings under seismic conditions (N_{cse}). These influences are footing width, slope angle, slope height, footing position, undrained shear strength and pseudo-static acceleration coefficient. As the number of parameters to be considered is high, a parametric study is conducted using FEM models. Obtained results are consistent with the results of available studies in literature. Proposed design charts allow the selection of problem specific N_{cse} values. A design procedure is defined and two design examples are presented for the calculation of the magnitude of undrained bearing capacity under seismic conditions.

1. Introduction

Design of shallow foundations requires the consideration of safety and serviceability. Safety check generally requires bearing capacity calculations, whereas serviceability calculations are done to keep the expected settlements within tolerable limits. However, a design that satisfies the serviceability criteria almost always satisfies the safety requirements. Then, the bearing capacity calculations are generally done for procedural purposes since they are compulsory in most design codes. But sometimes the combined influences of prevailing loading conditions and topography might reduce the bearing capacity of shallow foundations to critical levels and safety checks control geotechnical design. This is especially correct for the foundations of retaining structures, bridge abutments and transmission towers that rest on or near slopes within seismic zones. Under the influences of structural loads and earthquake accelerations, bearing capacity mechanism can induce slope instability which reduces the allowable bearing pressure in design. For projects that cover large distances, such as power transmission lines, many such foundations that support pylons and towers need to be designed. Thus, it is the goal of this study to develop simple design charts that allow the calculation of bearing capacity for different combinations of foundation dimensions, positions, soil properties, slope inclinations, crest heights and seismic accelerations. This study limits its scope to surficial shallow foundations resting on cohesive soils. The underlying reason for this preference is that sloping grounds generally have cohesive properties and the foundations of structures that are frequently built on sloping ground, such as retaining walls and transmission towers, are surficial shallow foundations. Accordingly, undrained behavior will be assumed as this corresponds to the most critical condition. Seismic loading will be defined using pseudo-static accelerations. Since there is no exact solution of the considered problem, it is essential to develop approximate solutions. For this purpose in this study, two-dimensional finite element method (FEM) is used for investigating the problem. As a shortcoming of the two-dimensional approach, modelled surficial foundations are always strip foundations. However, the applicability of the obtained results will be increased as the use of shape factors is adapted to seismic bearing capacity problems.

The problem of shallow foundations resting on or near slopes has attracted the attention of many researchers since late 1950s. These studies resulted in the development of several empirical equations and design charts [1–17,19,20]. Adopted methodologies of research are various and include limit equilibrium methods [6,7,15], upper bound [4,5,9,10,12,17,19] and lower bound analyses [20], method of stress characteristic [10,16], and finite elements method [8,10,16]. Additionally, recent studies used discontinuity layout optimization which

* Corresponding author.
E-mail addresses: ozer.cinicioglu@boun.edu.tr (O. Cinicioglu), aerkli@dbmetroyapim.com (A. Erkli).

https://doi.org/10.1016/j.soildyn.2018.04.027
Received 16 August 2017; Received in revised form 16 March 2018; Accepted 20 April 2018

is an upper bound limit state plasticity failure discretization scheme [13,14]. Yet, only a few studies consider the influence of seismicity and most of these emerged in the last two decades [7,12,15–20]. Among these, Sarma and Chen [15] studies slopes of cohesionless soils using limit equilibrium method. Similarly, Castelli and Motta [7] uses limit equilibrium method for studying the static and seismic bearing capacities of strip footings located situated near slopes. For this purpose, Castelli and Motta [7] assumes a circular failure mechanism and considers the influences of the sloping ground and soil inertia on bearing capacity using a pseudo-static approach. Georgiadis and Chrysouli [12], used an upper-bound plasticity solution for investigating the seismic bearing capacity of surficial strip footings on or near cohesive slopes. The kinematic mechanism proposed by Georgiadis [12] is extended for pseudo-static loading conditions by considering horizontal footing loads and the inertia of the soil body. On the other hand, Farzaneh et al. [20] employed finite element lower bound method to determine seismic bearing capacity of shallow foundations on cohesive slopes. Neglecting the changes to the geometry as the loading approaches collapse, the finite element lower bound models yielded lower bounds to the exact collapse load [20]. Among the studies that considered seismic bearing capacity of shallow foundations on or near cohesive slopes, Castelli and Motta [7], Farzeneh et al. [20] and Kumar and Rao [16] provided design charts, where Chrysouli and Georgiadis [12] provided an empirical equation based on the results obtained from the assumed kinematic mechanism.

To improve upon the existing literature, this study adopts a parametric approach employing numerical methods and deals with a more complete set of influences that control the behavior. These influences are soil strength, slope height, slope angle, seismic acceleration, soil strength, and foundation size and position relative to the slope. No single study in literature considered all of the above influences together for the ranges of variation examined in this study, therefore their practical applicability is relatively limited. The method of choice in this study is finite elements method since it allows the definition of different geometries and boundary conditions. This is especially important for the problem being considered as the mode of failure can change from a bearing capacity failure to slope instability as the material properties and geometrical conditions vary. Accordingly, in addition to the number and range of considered parameters, the novelty of the present study is that the combined influences of material properties, pseudo-static accelerations and problem configuration on the geometry of the failure mechanisms are considered with the use of FEM models.

Thus in this paper first the problem will be defined, followed by the presentation of the solution method. Then obtained results are compared with the results from available studies in literature and verified. Following, obtained results will be presented in the form of design charts. Then the results will be discussed and a design procedure is defined, followed by two design examples.

2. Definition of the problem and the details of the analyses

The problem of seismic bearing capacity of surficial foundations resting on or near cohesive slopes requires the consideration of a number of parameters and geometrical features. Changes in the configuration and geometry of the problem rather complicates the task of defining a general failure surface geometry. Finite element method requires no preliminary assumptions regarding the position and shape of the failure surface. This is especially important in case of footings located close to sloping ground as the mode of failure and its geometry is subject to change due to the combined influences of soil characteristics, problem geometry, and seismic accelerations. That is why finite element method which is a versatile tool that allows the consideration of different geometries is selected for this study. Furthermore, an important advantage of finite element over traditional limit equilibrium methods is that there is no need for the use of slices. This eliminates the need for assumptions regarding slice side forces as finite element

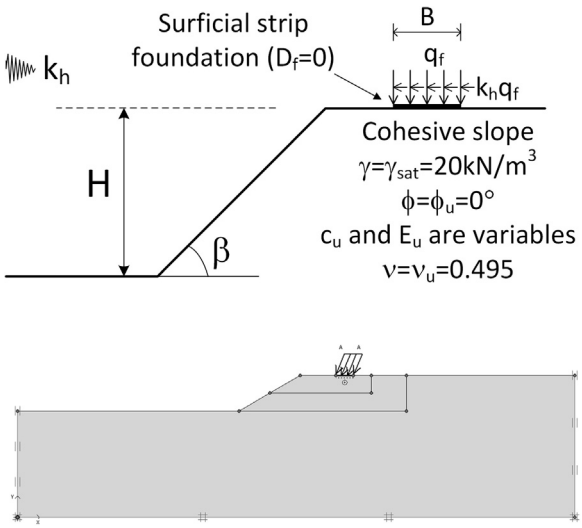

Fig. 1. General features of the problem and the corresponding model.

method preserves global equilibrium until failure state [21]. For this purpose, a commercial finite element software Plaxis 2D is used. Graphical representation of the problem and the corresponding model are illustrated in Fig. 1. Several assumptions were made towards the development of the model. Plane-strain conditions are assumed and the study considers surficial strip foundations. Therefore the influence of embedment on bearing capacity is ignored. The footing is represented by a rigid plate element and the interface is assumed to be rough. Pseudo-static approach is preferred for defining seismic effects and it is assumed that the inertia force of the structure acts at the base of the footing. Therefore, any moments due to inertia effects are neglected. A holistic pseudo-static approach is chosen in which horizontal seismic acceleration coefficients (k_h) used for calculating the inertia forces of the structure and the slope are assumed to be equal. By definition, seismic acceleration coefficients correspond to the ratio of seismic acceleration over gravitational acceleration (g). Moreover, horizontal accelerations ($k_h g$) are uniform throughout the entire model subjecting it to constant inertial forces. However, vertical component of the seismic acceleration is ignored ($k_v = 0$) owing to its insignificant influence on seismic bearing capacity [22]. Soil behavior is modelled as elastic – perfectly plastic with a Tresca failure criterion. Additionally, as illustrated in Fig. 1, slope and soil underlying it are uniform and soil properties do not vary with depth.

Seismic bearing capacity ($q_{ult,se}$) is defined using an appropriate seismic bearing capacity factor (N_{cse}) as shown in Eq. (1).

$$q_{ult,se} = N_{cse} c_u \tag{1}$$

Here, the value of N_{cse} is dependent on the collective influences of all variables and problem geometry. Considering that the measurement of undrained shear strength of cohesive soils is a straightforward task, the only requirement for the calculation of $q_{ult,se}$ is the determination of N_{cse}. Thus, the goal of this study is to prepare design charts for the selection of the value of N_{cse}. The first step in the development of design charts is the identification of influential factors. Following, the problem is solved numerically using different combinations of influential factors and obtained results are presented graphically for simplicity. Accordingly, factors that are defined as variables can be categorized into three groups. First group mainly involves factors that define the geometry of the problem. Geometry of the problem requires the definition of slope geometry, footing width and the position of the footing. Factors that define the geometry of the slope are height (H) and inclination (β). However by examining Fig. 1 it is possible to deduce that the influence of H on $q_{ult,se}$ must be measured relative to the width of the footing (B). So knowing the magnitudes of H/B and β is sufficient to define the

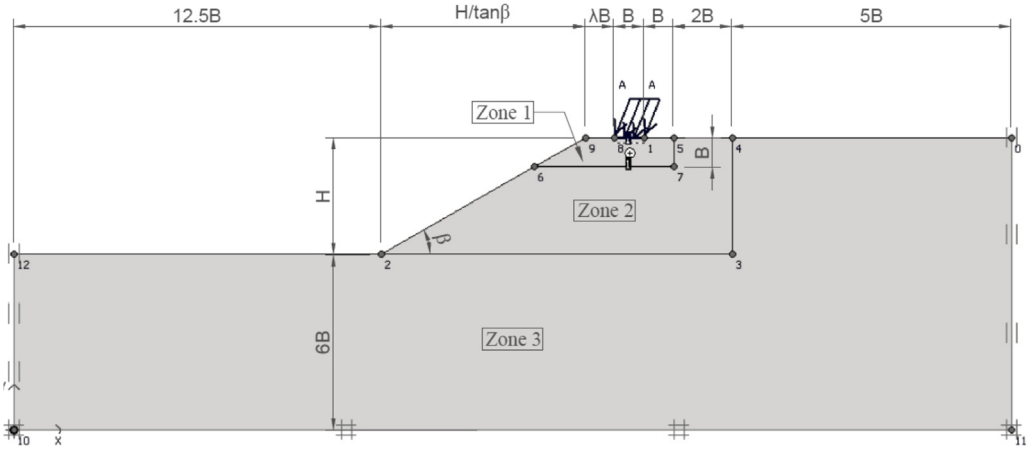

Fig. 2. Dimensions of the FEM Model.

geometry of the slope. Therefore, it is possible to keep the value of B constant as its influence on $q_{ult,se}$ is relative to H. The fixed value used for B is 2 m. Then, parametric analyses were conducted for the following values: 0, 1, 2 and 4 for H/B and 0°, 15°, 30° and 45° for β. Evidently, whenever H/B is 0, so is β, or vice versa. Moreover, a normalized distance (λ) is used to quantify the position of the foundation with respect to the crest of the slope as illustrated in Fig. 1. λ is the distance between the footing's near edge and the crest of the slope normalized with B. Magnitudes of λ used in the analyses are 0, 0.5, 1 and 2. Additionally, analyses with λ values other than these have also been conducted to accurately identify the magnitude of threshold λ at which the influence of slope on bearing capacity diminishes. Second group of factors define the state of the soil. Since Mohr-Coulomb elastic-perfectly plastic constitutive model is used with total stress undrained parameters, it is necessary to define only undrained shear strength (c_u) and undrained stiffness parameters. However, since the problem focuses on the perfect plastic failure of the system, undrained stiffness (E_u) is taken as a function of c_u. Accordingly, in this study $E_u = 200c_u$. Undrained Poisson's ratio (υ_u) should theoretically be equal to 0.5 to simulate fully incompressible behavior, but this leads to singularity of the stiffness matrix. To avoid numerical problems caused by an extremely low compressibility, υ_u is taken as 0.495. Additionally, the range of values for the soil unit weight (γ) is rather limited and its influence on the results is insignificant. So, soil's saturated unit weight is kept constant at 20 kN/m^3. Selected values of c_u for the cohesive slope soil are 25, 50, 100, 200 kPa, corresponding to soft, stiff, very stiff and hard consistencies of clay, respectively. Using the selected fixed values of γ and B, dimensionless soil strength is defined using $c_u/(\gamma B)$. As a result, values of $c_u/(\gamma B)$ used in the parametric analyses are 0.625, 1.25, 2.5, and 5. The third and the last group of factors defines the earthquake effect. Since the approach is pseudo-static, vertical and horizontal components of earthquake accelerations are considered to act as static accelerations. As explained above, vertical component of acceleration is not considered due to its insignificant influence on the problem, thus $k_v = 0$. On the other hand, horizontal seismic acceleration coefficient (k_h) takes the following values: 0, 0.1, 0.2, 0.3, and 0.4. As a result, seismic bearing capacity factor as a function of dimensionless parameters affecting the stability of the system is defined as:

$$N_{cse} = f\left(\frac{H}{B}, \beta, \lambda, \frac{c_u}{\gamma B}, k_h\right) \tag{2}$$

Surficial strip footing is represented by a rigid plate element in the FEM model. The plate element is assumed to be a weightless elastic material. For all analyses, footing axial stiffness (EA) is $3\times10^7 kN/m$, flexural stiffness (EI) is $2.5\times10^6 kNm^2/m$, equivalent plate thickness (d_{eq}) is $1.0m$, and Poisson's ratio (ν) is 0.2. The footing is assumed to be fully rough. Accordingly, an interface was defined below the plate and interface strength reduction factor (R_{inter}) is specified as unity in all different soil data sets.

3. FEM model

General geometry of the problem to be modelled is shown in Fig. 1. Consideration of all combinations of the different geometrical features (β, H, λ) defined in the previous section, requires the development of numerous FEM models. For all these FEM models with different geometries, it is essential to make sure that the problem is not influenced by the position of outer boundaries. For this purpose, model dimensions incrementally increased until the boundary effects disappeared. Resulting model geometry for which there are no boundary effects is shown in Fig. 2. Standard fixities are used at the boundaries in the form of horizontal fixities at the sides and total fixities at the bottom of the model (Fig. 2). The position of the right boundary relative to the foundation is defined as a function of the width of the foundation (B). On the other hand proximity of the left boundary to the bottom edge of the slope is set at $12.5B$ for all models. Additional, bottom boundary is always $6B$ below the bottom edge of the slope. These generic model dimensions prevent the boundaries from influencing the analyses' results.

Considering the large number of models to be solved, generated meshes are optimized to keep the use of computer memory and computational time at an acceptable level. This is achieved by following the methodology of Georgiadis [8]. Georgiadis [8] divided the model into several zones and used finer meshing for the zones that experience higher deformation. As a result, the model is divided into three regions depending on mesh density. The first zone (zone 1) just below the foundation corresponds to the region within which the deformations due to bearing type of failure take place. Since it is reported in literature that increases in horizontal acceleration results in shallower bearing failure mechanisms [19,23,24], the depth of zone 1 is equal to the width of the foundation (B) which is equal to the depth of the bearing capacity mechanism under static conditions. Similarly right boundary of zone 1 away from the slope is again equal to B following the same reasoning. Bottom boundary of the second zone (zone 2) is defined based on the vertical position of the slope's toe and its boundary away from the slope is $3B$ away from the corner of the foundation. Finally, all the remaining regions are considered as zone 3. Mesh refinement exercises were done to obtain the extent of necessary mesh refinement in these zones. Accordingly at the selected mesh density, global coarseness of the mesh is initially set to "fine". Then regions 1 and 2 which are respectively closer to the foundation are refined once. Following, region 1 which is just below the foundation is refined once more. Finally, the corners of the foundation is selected for further refinement. Resulting

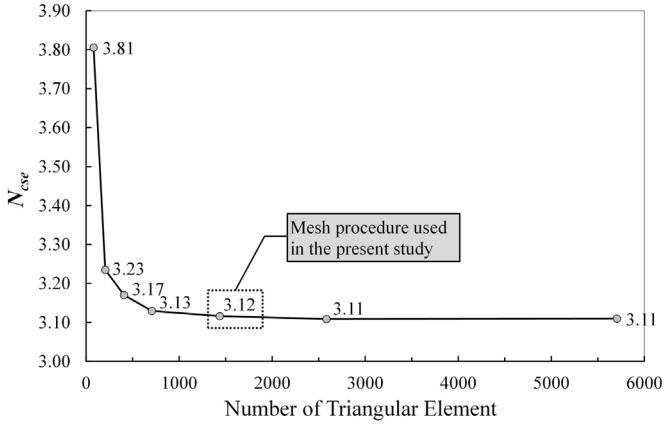

Fig. 3. Variation of N_{cse} with the number of triangular elements ($\beta = 30^{\circ}$, H = 4.0m, $\lambda = 0$, $c_u = 100$kPa, $k_h = 0.2$).

form of the adopted mesh corresponds to the optimum condition which yields correct results with manageable computational times. Considering the final state of the model mesh, the number of soil elements for a model is approximately 1600. The average areas of triangular mesh elements are roughly 2.4 m^2 for zone 3, 0.15 m^2 for zone 2, and 0.02 m^2 for zone 1. As shown in Fig. 3 for a selected set of variables, calculated N_{cse} value has converged quite well to its limit value by following the defined mesh generation procedure. Apparently, N_{cse} value obtained by the selected meshing procedure is approximately the same as the limit N_{cse} value. Furthermore, the number of elements used in the defined mesh density is one quarter of that used by the mesh that yields the limiting N_{cse} value (Fig. 3).

As bearing capacity type of failure is the most prominent failure mode for the problem being considered, it is necessary for the resulting model to capture that behavior closely. Therefore, undrained static bearing capacity problem of strip footings on level ground is used as benchmark. Evidently, the exact solution to this problem is well known [25]. After employing a trial and error method during which the dimensions of different refinement zones are varied, value of the bearing capacity factor (N_c) that is closest to the exact value ($\pi + 2 = 5.14$) is obtained as 5.16. The difference between the exact and obtained values is just 0.4% which is acceptable. Furthermore, the failure mechanism obtained is identical to the mechanism proposed by Prandtl [25].

Brinkgreve et al. [26] reported that failure loads in bearing capacity calculations are generally overestimated when 6-node elements are used. That is why the FEM mesh of this study uses 15-node triangular elements even though they consume more memory and computational time relative to 6-node triangular elements.

Each test has three calculation phases following the initial phase. In the initial phase, geostatic stresses in the model are generated using gravity loading option as K_o procedure is only applicable to models with horizontal ground surfaces. Following the initial phase, loads from the superstructure are activated. However, in order to prevent the slope from failing prematurely without measuring the seismic bearing capacity, bearing pressure is applied vertically as unity at the foundation level. Since the problem being considered is seismic, in addition to the vertical component of bearing pressure (q) there will be a horizontal component due to the inertia of the superstructure and foundation system. Accordingly, the inertia force at the foundation level is defined as $k_h q$ in the direction of the slope which corresponds to the most unfavorable condition. The initial magnitude of $k_h q$ is insignificant when q is unity for a stable system, thus the application of the resultant pressure with components vertical q and horizontal $k_h q$ prior to pseudo-static analysis does not influence the results. Then in the second phase following the initial phase, horizontal acceleration (k_h) is imposed on the model by changing the value of the acceleration multiplier to one. Changing the value of acceleration multiplier to one will activate k_h which has been identified in the model preparation stage. The direction of pseudo-static acceleration is selected to act towards the slope which will result in the inertia of the slope to act as a driving force. Finally, in the last phase of calculation, a multiplier for the bearing pressure is input which will incrementally increase the inclined bearing pressure until model fails. Using the value of multiplier that corresponds to failure, seismic bearing capacity ($q_{ult,se}$) can be obtained. Then following the relationship defined in Eq. (1), N_{cse} value can be directly calculated. The details of the model, calculation stages and the settings are explained in detail in Erkli [27].

4. Comparison of the results with previous studies

The results obtained in this study are compared with the studies of other researchers that worked on similar problems. The problem being considered requires the evaluation of many different configurations regarding the position of the foundation (on or a distance away from the crest of the slope) and loading conditions (static or seismic). That is why available studies in literature focused on different aspects of the problem. These studies and their results are used as benchmarks to validate the results of the present study. Previous studies on the topic can be divided into six groups based on the presence and position of the foundation on the slope and the impact of seismic acceleration. The simplest configuration for the problem under consideration corresponds to the case of static stability of a cohesive slope. Taylor [28] studied the problem of cohesive slope stability and defined the limiting slope height (H_{cr}) as a function of c_u, γ, and a non-dimensional stability number m.

$$H_{cr} = \frac{c_u}{\gamma m} \tag{3}$$

For cases when $\beta \geq 53^{\circ}$, m increases linearly with β independent of the depth of the hard stratum (D) from the ground surface. For cases when $\beta < 53^{\circ}$, value of m is a function of both β and D. Moreover, for the cases where $\beta < 53^{\circ}$ and $D = \infty$, m is always equal to 0.181 [29]. Since this combination of β and D applies to all models of this study, consistent with Taylor [28], slope heights of the models (H) that failed in the first calculation phase (slope failure under static conditions) are all greater than H_{cr} ($=c_u/[0.181\gamma]$).

The second calculation phase of the model involves the seismic stability of the cohesive slope as horizontal pseudo-static acceleration is imposed. Koppula [30] developed design charts that allow the calculation of factor of safety of slopes ($F.S.$) using Eq. (4) given below.

$$F.S. = \frac{a_o}{\gamma} N_1 + \frac{c_o}{\gamma H} N_2 \tag{4}$$

where N_1 and N_2 are stability numbers, a_o is the increase in c_u with depth and c_o is equal to c_u at the top of the slope. Stability numbers N_1 and N_2 are functions of k_h, β, and D. Clearly in this study $a_o = 0$ and $c_o = c_u$. Therefore, H_{cr} under pseudo-static conditions can be calculated as $c_u N_2/\gamma$ where N_2 is obtained from design charts provided by Koppula [30]. When investigated, it was observed that for all models that failed in the second phase of the calculation (seismic instability of the cohesive slope) slope height is equal to or greater than H_{cr}. The results for the barely stable and failing slopes are given in Erkli [27]. Accordingly, the results of this study are consistent with the findings of Koppula [30].

The third and final calculation phases of the models involve failure due to the imposed loading from the foundation. At this calculation phase, failure occurs as a result of bearing capacity failure. The mode of failure is a function of constitutive properties of the soil, imposed acceleration and the geometry of the problem. However, it should be pointed out that slope instability is not the only failure type that is observed in the third calculation phase. As a result of the application of k_h, sliding failure can occur at the soil-foundation interface. This will be discussed in the following parts. A method for the prediction of the possible mode of failure will be defined in the subsequent sections.

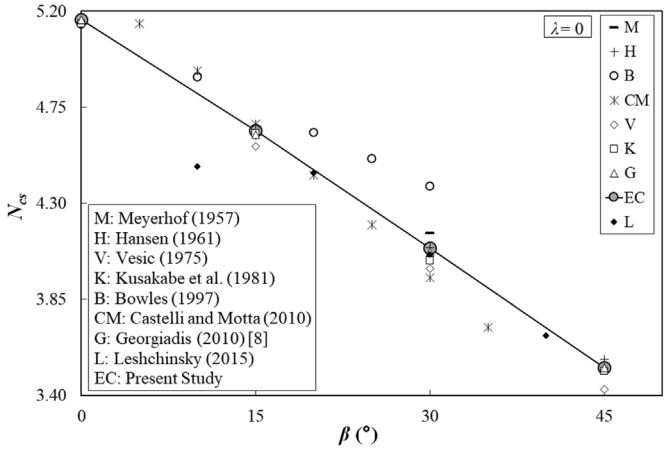

Fig. 4. Comparison of N_{cs}–β relationships obtained in this study with previous studies (for λ = 0 and $c_u/\gamma B$ = 5).

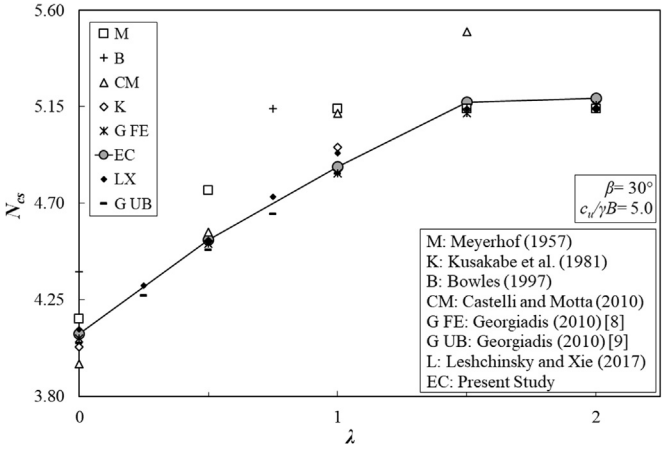

Fig. 5. Comparison of N_{cs}–λ relationship obtained in this study with previous studies (for β = 30°and $c_u/\gamma B$ = 5).

Studies in literature that are comparable to the failure modes observed in this phase are divided in to four groups. These groups are defined according to the presence of seismic acceleration (static or seismic) and the position of the foundation on the slope ($\lambda = 0$ or $\lambda > 0$).

The first comparison is made with studies for which $k_h = 0$ and $\lambda = 0$. The variation of static bearing capacity factor (N_{cs}) with β is compared with the findings of other researchers. An example for this comparison is given in Fig. 4 for $c_u/\gamma B = 5$. Results of the present study showed perfect agreement with all studies compared, except the ones proposed by Bowles [6] and Castelli and Motta [7]. Bowles [6] assumes that bearing capacity type of failure will prevail in all cases. Accordingly the approach of Bowles [6] requires that the reduction in N_{cs} must be proportional to the reduction in the length of the assumed failure mechanism due to the presence of a nearby slope. As a result, in cases where the mechanism deviates from general bearing type of failure, Bowles [6] overestimates N_{cs}. On the other hand, Castelli and Motta [7] used limit equilibrium method of slices and assumed circular failure surfaces that start from the edge of the footing and continue until reaching the slope surface. The differences between the actual and these assumed failure surface geometries results in the deviation of the calculated N_{cs} values as observed in Fig. 4.

In cases where the foundation is located at a distance from the crest of the slope, influence of λ over N_{cs} should be considered as well. Therefore comparisons with the studies of previous researchers is done by fixing the values of β and $c_u/\gamma B$. An example of this comparative study is shown in Fig. 5. As expected, N_{cs} increases as λ increases. The increase of N_{cs} continues until the threshold value of λ beyond which N_{cs} is equal to the static bearing capacity factor for horizontal ground. In other words, threshold λ corresponds to the distance at which the influence of slope diminishes. Results found for all normalized footing distances indicate a good agreement with those of Kusakabe et al. [4] and Georgiadis [8,9]. Apparently, Castelli and Motta [7] yields unrealistically high factors. On the other hand, the threshold λ values are smaller in case of Meyerhof [1] and Bowles [6] since these researchers used assumed failure surface geometries, unlike the FEM analyses of this study and Georgiadis [8].

Comparisons for the seismic condition are similarly grouped according to the position of the footing on the slope. However, as a result of the inertia effect, seismic bearing capacity factor (N_{cse}) is influenced by the height of the slope (H) as well. An example of the comparison with other researchers made for footings located on the edge of the slope is shown in Fig. 6. Here, Kumar and Rao [16] used the method of stress characteristics with a semi-infinite slope assumption. Therefore,

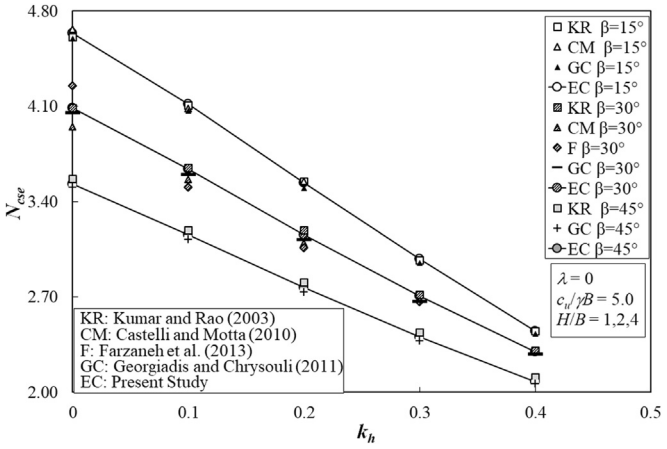

Fig. 6. Comparison of the N_{cse} values given by different researchers for various k_h, β, and H/B combinations (for λ = 0 and $c_u/\gamma B$ = 5).

results of Kumar and Rao [16] are relevant only for the conditions when $\lambda = 0$. On the other hand, Farzaneh et al. [20] used finite element lower bound method. The preference of lower bound is to assure that the results are always on the safe side. Moreover Farzaneh et al. [20] considered only bearing capacity type of failure and kept the value of H/B constant at 4. Additionally, Georgiadis and Chrysouli [12] studied undrained seismic bearing capacity of shallow foundations on slopes using upper bound method. Using the kinematic mechanism proposed by [9], Georgiadis and Chrysouli [12] extended the mechanism to include the influences of horizontal footing loads and inertial loads. However, upper bound solution discussed in [12] does not consider the influence of slope height on the governing failure mechanism. Based on the results obtained from the upper bound ultimate load calculations, Georgiadis and Chrysouli [12] proposed an empirical equation for calculating the ultimate load of footings situated at the crest of a slope. Even though the design charts provided by [7,16,20] and the empirical equation proposed by [12] are relatively limited in extent, they provide valuable contribution to check the validity of the present study. Evidently, results of [7,12,16,20] and present study are very similar as shown in Fig. 6.

Final comparison is made for the seismic condition when $\lambda > 0$. An example of the comparison is shown in Fig. 7. Clearly, results of the present study lies in between the values given by the other researchers.

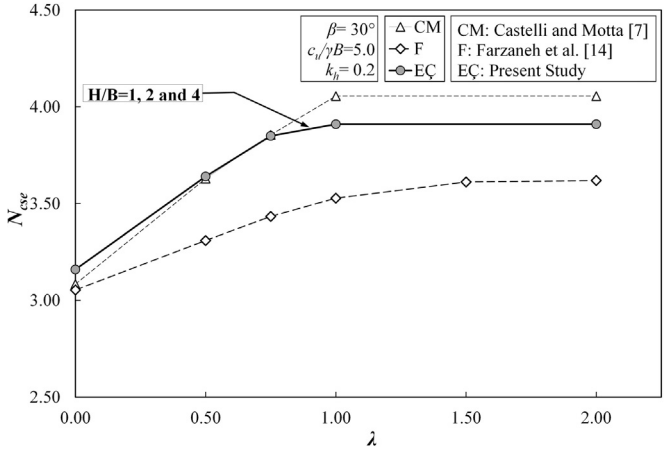

Fig. 7. Comparisons of the N_{cse}–λ relationships with the results of other researchers (for β = 30°, k_h = 0.2, and $c_u/\gamma B$ = 5).

As expected, N_{cse} values obtained in the current study are greater than the ones proposed in the study by Farzaneh et al. [20] which used a lower bound approach. On the other hand, values given by Castelli and Motta [7] are dependent on the validity of the assumed failure mechanism as discussed previously. As a result, it can be concluded that the results of the present study compare well with other studies. Moreover, FEM satisfies both equilibrium and compatibility requirements within numerical approximation. Therefore, different than the classical upper and lower bound techniques, FEM calculated failure loads are not dependent on the admissibility of the defined failure mechanisms.

5. Examination of failure mechanisms

From the analyses of model results, it is noted that there are four principal failure modes for the footing on cohesive slope problem. The first failure mode is overall slope failure which initiates well behind the edge of the footing and creates a failure mechanism that covers the entire model. In case of overall slope failure, defined geometry with given material properties is not stable under imposed accelerations, whether these accelerations are gravitational or pseudo-static. Cohesive slope failure was defined by Taylor [28] for static conditions and by Koppula [30] for seismic conditions as explained above. As the accelerations are pseudo-static, even models with horizontal grounds can experience overall slope failure if the accelerations are sufficiently high. Under the influence of constant and uniform pseudo-static accelerations, a model with a horizontal ground surface behaves the same way as a model with a ground inclination equal to $\beta = \tan^{-1}[k_h/(1-k_v)]$ behaves under static conditions. Then if the model is unstable under the imposed accelerations, overall slope failure commences. For such models failure surfaces extend all the way to model boundaries since soil strength is uniform. Increasing the model boundaries only increases the size of the failing wedge as the overall system is unstable under the imposed accelerations. The conditions under which overall slope failure is observed conform to the results of Taylor [28] and Koppula [30].

The second failure mode is called foundation failure. Foundation failure corresponds to bearing capacity failure. Foundation failure occurs in the final phase of the analyses and the resulting failure surface initiates just below the footing edge as illustrated in Fig. 8 for $\lambda = 0$ and in Fig. 9 for $\lambda > 0$. The failure surface might extend all the way to the slope surface or might end at the top ground surface if the footing is located sufficiently away from the crest of the slope. This is similar to the failure mode characterization made by Meyerhof [1] and Georgiadis [8].

Third failure mode is slope instability initiated by the foundation load. In this failure mode (Fig. 9), under the imposed accelerations the slope is barely stable and when the foundation loads are imposed slope fails. The failure surfaces extend beyond the toe of the slope (Fig. 10). Since the resistance provided by the barely stable slope is smaller than the capacity of the system against bearing failure, calculated seismic bearing capacity factors are relatively smaller than the values expected from the system. The impact of foundation instability on seismic bearing capacity will be explained when the design charts are presented.

Fourth failure mode is foundation sliding. For those models with stable slopes, foundation slides if $k_h \geq 0.36$. The threshold value of k_h for foundation sliding is 0.36 since at this k_h value horizontal component of the bearing pressure at failure ($q_{ult,se_h} = q_{ult,se} \times k_h$) becomes equal to the undrained strength of the soil (c_u) at the fully rough interface of the rigid foundation as defined in FEM models. This condition is defined by multiplying both sides of Eq. (1) as shown below.

$$q_{ult,se_h} = c_u N_{cse} k_h \tag{5}$$

Accordingly, a fully rough foundation will slide when $N_{cse} k_h$ is unity. As explained by Richards *et al.* [31] with dynamic fluidization theory, as the horizontal acceleration intensity increases during a dynamic event, the active thrust increases, the passive thrust decreases, and the wedge angles of the failure mechanism become progressively smaller. Thus the failure wedge becomes confined to a shallower depth. Shallower failure mechanisms correspond to smaller N_{cse} values. Accordingly, there is an inverse relationship between k_h and N_{cse} as illustrated

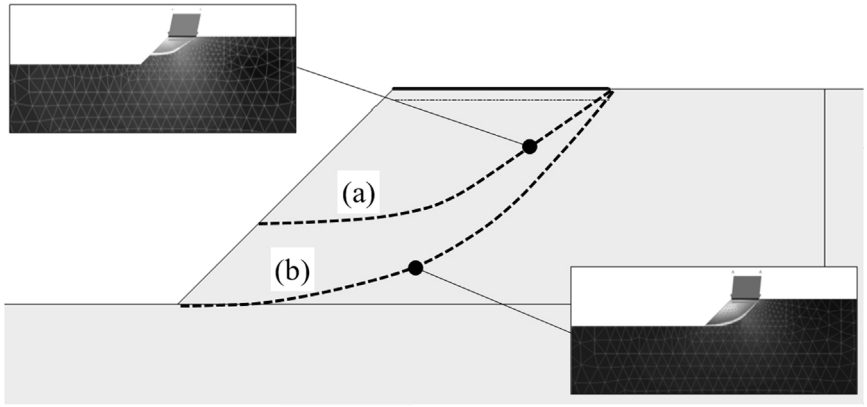

Fig. 8. Typical foundation failure modes for λ = 0 condition and corresponding FEM output examples (a) β = 45°, H/B = 1, $c_u/\gamma B$ = 1.25, k_h = 0.2; (b) β = 45°, H/B = 1, $c_u/\gamma B$ = 0.625, k_h = 0.1.

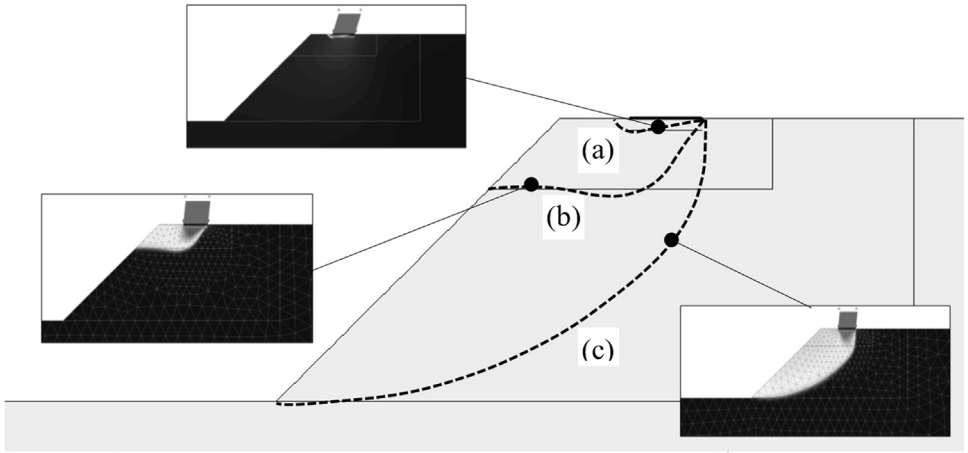

Fig. 9. Typical foundation failure modes for $\lambda > 0$ condition and corresponding FEM output examples (a) $\beta = 45^{\circ}$, H/B = 4, $c_u/\gamma B = 2.5$, $k_h = 0.3$; (b) $\beta = 45^{\circ}$, H/B = 4, $c_u/\gamma B = 2.5$, $k_h = 0.1$; (c) $\beta = 45^{\circ}$, H/B = 4, $c_u/\gamma B = 1.25$, $k_h = 0.1$.

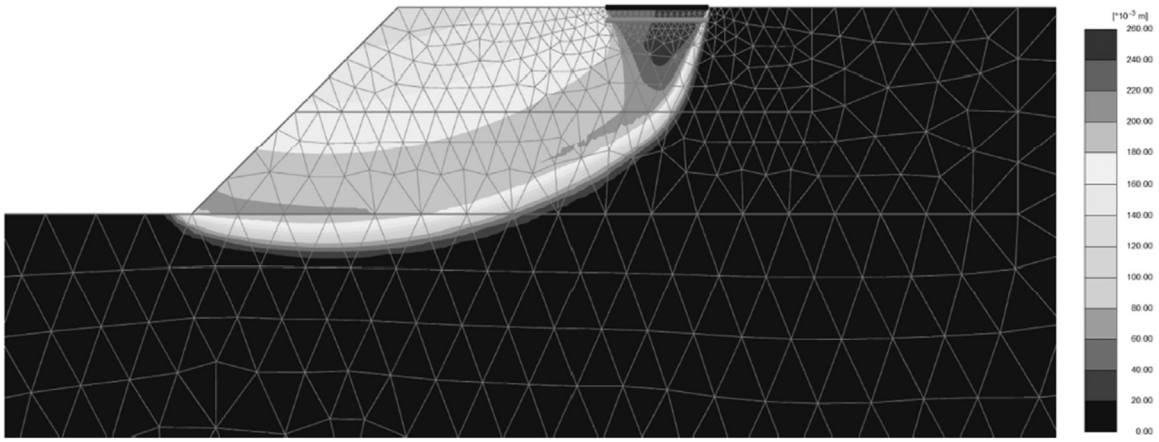

Fig. 10. Foundation caused slope instability ($\beta = 45^{\circ}$, $H/B = 2$, $\lambda = 2$, $c_u/(\gamma B) = 0.625$, $k_h = 0$).

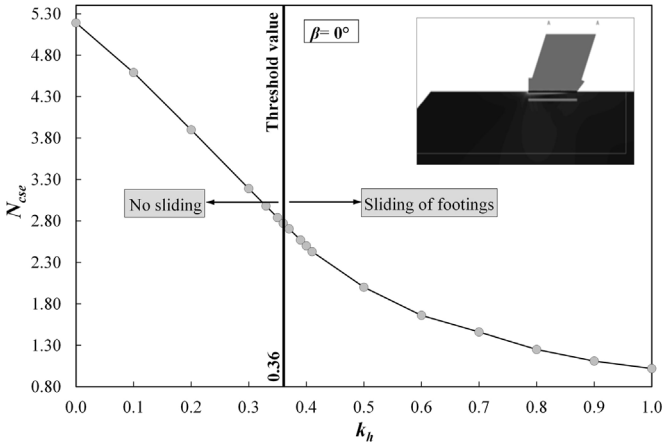

Fig. 11. Variation of N_{cse} with k_h for level ground and an example of analysis failure by foundation sliding ($\beta = 45^{\circ}$, H/B = 4, $\lambda = 2$, $c_u/\gamma B = 2.5$, $k_h = 0.4$).

in Fig. 11 for level ground. For any value of $k_h \geq 0.36$, $N_{cse} k_h = 1$, corresponding to foundation sliding mode of failure. The assumption of a fully rough interface is an appropriate assumption since even a small amount of foundation embedment improves sliding resistance. So it is correct to define the interface as fully rough to prevent the underestimation of lateral resistances.

As explained in the preceding section, in case of FEM models that fail with slope instability, Eq. (4) proposed by Koppula [30] also predicts slope failure. Additionally, models for which $k_h \geq 0.36$ fail by sliding at the soil-foundation interface. Therefore, it can be established that any model which does not fail with sliding or slope instability, will fail with bearing capacity mode.

6. Proposed design charts

Seismic bearing capacity of a strip footing can be calculated using Eq. (1) as long as the appropriate values of c_u and N_{cse} are known. Value of c_u can be obtained by testing, whereas determining the value of N_{cse} requires the consideration of the influences of H/B, β, λ, $c_u/\gamma B$, k_h as defined in Eq. (2). Accordingly, the goal of this study is to develop a solution method that can be easily implemented by geotechnical designers or practitioners. For this purpose design charts shown in Fig. 12 to Fig. 14 are developed. The special case of level ground is given in Fig. 11 as corresponding H/B and β values are zero. Combinations for the conditions that are not shown in Fig. 12, Fig. 13, and Fig. 14 correspond to sliding or slope failure states.

Evident from the design charts, shapes of the $\lambda - N_{cse}$ relationships are generally similar. Value of N_{cse} increases almost linearly with the increase in λ until the threshold λ beyond which the influence of the slope diminishes (λ_o) is reached. However for certain β, H/B, $c_u/(\gamma B)$ and k_h combinations the trends of the $\lambda - N_{cse}$ relationships are different; N_{cse} initially rises rapidly for a slight increase in the distance of the foundation from the crest of the slope, then the rate of rise in N_{cse} drops significantly. For these slopes, λ_o is also significantly higher. The reason

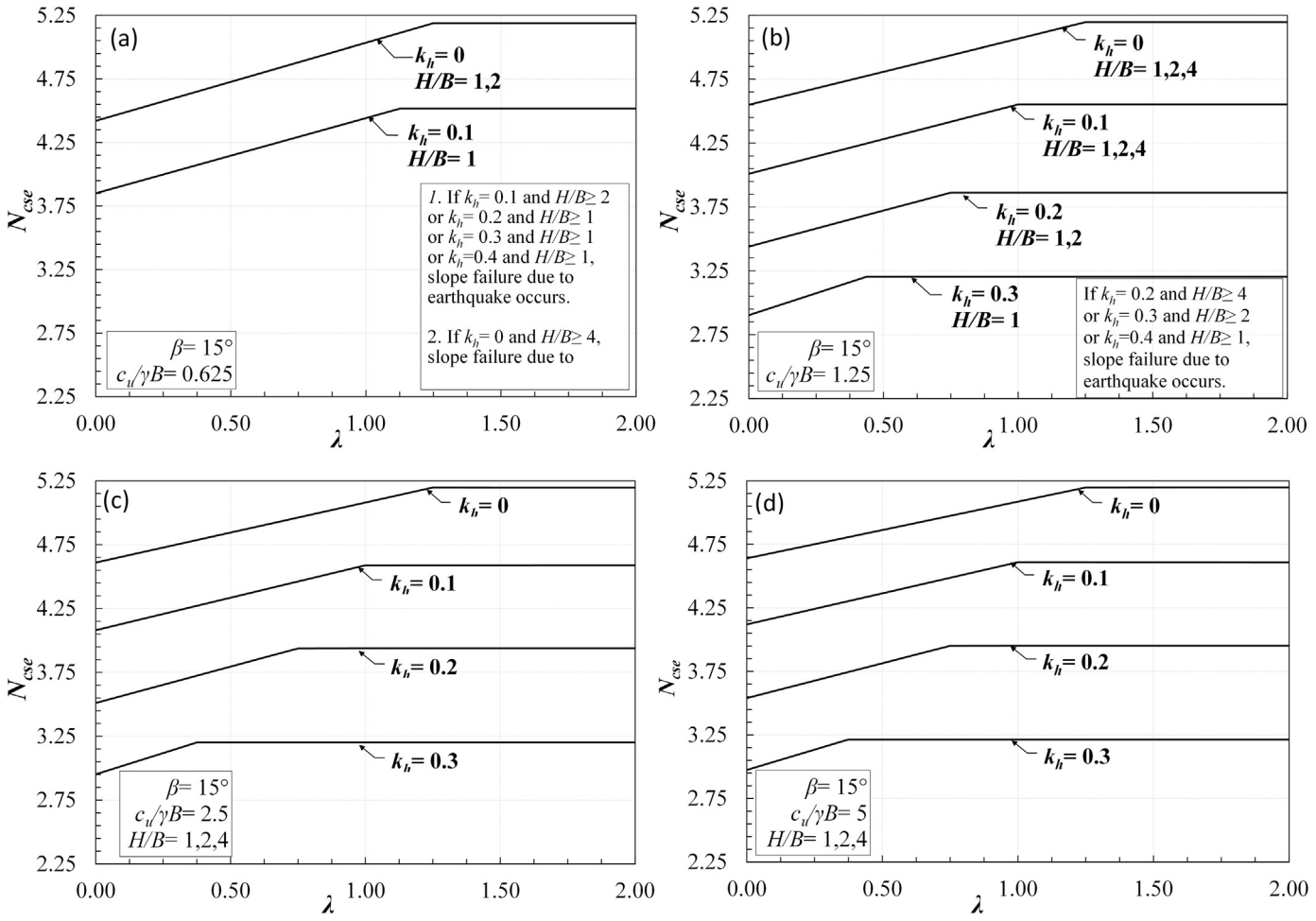

Fig. 12. Design charts for seismic bearing capacity factor of surficial strip footings located near cohesive slopes with β = 15° and H/B = 1, 2, 4 (a) $c_u/\gamma B$ = 0.625, (b) $c_u/\gamma B$ = 1.25, (c) $c_u/\gamma B$ = 2.5, (d) $c_u/\gamma B$ = 5.

for such response is that these slopes are barely stable and as λ increases failure mode changes from bearing capacity failure to foundation caused instability. Since these slopes are barely stable, λ_o is also significantly greater. Fig. 15 illustrates the changes in the prevailing failure mechanism as λ of the foundation on barely stable slope increases. As shown in Fig. 15, failure mechanism is foundation failure until approximately $\lambda = 0.6$. Then until the threshold $\lambda = \lambda_o = 7$, slope fails under the imposed foundation loads. $\lambda - N_{cse}$ relationship for the stable slope with $H/B = 4$ is provided in Fig. 15 for comparison.

A design procedure for calculating the value of N_{cse} based on the design charts presented in this study is proposed with the following steps:

- Variables defining geometrical (H/B, β, λ), material ($c_u/\gamma B$) and loading characteristics (k_h) of the problem under consideration are identified.
- Expected failure mode of the problem is obtained:
  - o Use Eq. (4) with the charts proposed by Koppula [30] to check the possibility of overall slope failure.
    - If the calculated $F.S. \geq 1$
      - Failure is caused by the foundation for $k_h < 0.36$.
      - Failure mode is sliding for $k_h \geq 0.36$.
    - If the calculated $F.S. < 1$, then the failure mode is overall slope failure.
- If failure is caused by foundation loads, then select and use the appropriate chart or charts given in Fig. 12, Fig. 13, and Fig. 14. Use interpolation and extrapolation as necessary.

Erkli [27] provides design examples for different combinations of H/B, β, λ, $c_u/\gamma B$, and k_h. Several of these design examples involve both interpolation and extrapolation to obtain the appropriate value of N_{cse}. For verification purposes, Erkli [27] compares the values of N_{cse} obtained using the outlined design procedure with the values obtained from the finite element model analyses simulating the same conditions. The results are consistent with each other for all conditions. Two such examples are provided here:

Example 1: Characteristics of the problem are given as following; $B = 1.5m$; $H = 6m$; $\beta = 30°$; distance of the footing from the edge of the slope = 1.2 m; $\gamma = 20kN/m^3$; $c_u = 75kPa$; $k_h = 0.15$. Accordingly, parameters given in Eq. (2) are found; $H/B = 4$; $\lambda = 0.8$; $c_u/\gamma B = 2.5$. Using Eq. (4) with the charts provided by Koppula [30], $F.S.$ against seismic slope instability for the given conditions is 1.3. Additionally, $k_h = 0.15 < 0.36$, therefore foundation will not slide. The expected mode of failure is foundation failure and proposed design charts can be used. Since $k_h = 0.15$ is between the values used to prepare the design curves, linear interpolation is used between the curves for $k_h = 0.1$ and $k_h = 0.2$ given in Fig. 13c. The value of

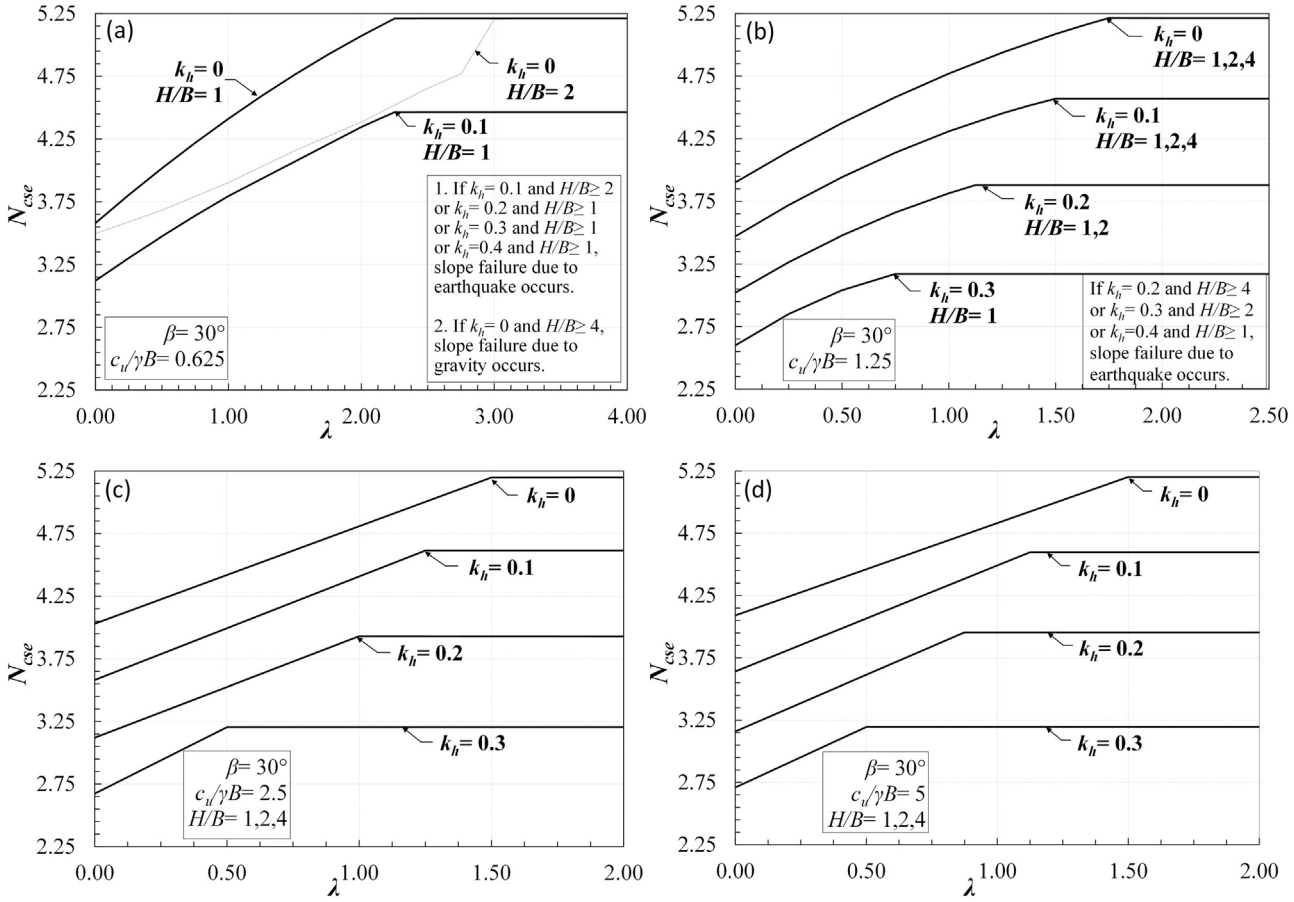

Fig. 13. Design charts for seismic bearing capacity factor of surficial strip footings located near cohesive slopes with β = 30° and H/B = 1, 2, 4 (a) $c_u/\gamma B$ = 0.625, (b) $c_u/\gamma B$ = 1.25, (c) $c_u/\gamma B$ = 2.5, (d) $c_u/\gamma B$ = 5.

N_{cse} calculated by linear interpolation is 4.01. Then, using Eq. (1) with $c_u = 75kPa$, $q_{ult,se}$ is calculated to be 301 kPa. The problem with the same characteristics is modelled using FEM and $q_{ult,se}$ is found to be 309kPa. Clearly, estimated seismic bearing capacity via linear interpolation is on the safe side and the difference between the results is only 2.6%.

Example 2: Characteristics of the problem are given as following; $B = 2m$; $H = 8m$; $\beta = 60°$; distance of the footing from the edge of the slope = 0 m; $\gamma = 20kN/m^3$; $c_u = 200kPa$; $k_h = 0.1$. Accordingly, parameters given in Eq. (2) are found; $H/B = 4$; $\lambda = 0$; $c_u/\gamma B = 5$. Expected failure mode is evaluated using Eq. (4) with design charts provided by Koppula [30]. The stability number N_2 that corresponds to the combination of $\beta = 60°$ and $k_h = 0.1$ is obtained from the charts Koppula [30] provided as 4.8. Since $a_o = 0$, then $F.S. = 5.76$ against slope instability. Additionally, $k_h = 0.1 < 0.36$, therefore foundation will not slide. Thus, the expected mode of failure is foundation failure. The problem requires extrapolation. For this purpose, N_{cse} is obtained for conditions with the same characteristics but different β values. The results are shown in Fig. 16. Clearly, N_{cse} linearly varies with β and the value of N_{cse} is calculated as 2.69 for the problem at hand. Then, using Eq. (1), $q_{ult,se}$ is calculated as 538kPa. The same problem is also modelled using FEM. As expected, failure mode is foundation failure with a bearing capacity equal to 540kPa. As a result, estimated bearing capacity via linear extrapolation is on the safe side and the difference between the results is less than 1%.

7. Discussions

As identified in the preceding sections, five parameters influence the magnitude of N_{cse}. These are k_h, β, λ, H/B, and $c_u/\gamma B$. When the results of finite element models conducted in this study are analyzed, it is noticed that there is an inverse relationship between k_h and N_{cse} (Fig. 17) as expected. Clearly, $k_h - N_{cse}$ relationship is influenced by the geometry of the problem. As the magnitude of λ increases, the influence of the slope on $k_h - N_{cse}$ relationship reduces. However, this effect is independent of the value of H/B. Similarly, for the slope angle β to have any influence on the magnitude of N_{cse}, λ should be less than the problem specific threshold value. The threshold value for the normalized footing distance is shown by λ_o. For $\lambda \leq \lambda_o$, increasing values of β results in smaller N_{cse} values as shown in Fig. 18. Additionally, greater λ values correspond to greater magnitudes of N_{cse} until λ_o as evidenced by the results in Fig. 12, Fig. 13, and Fig. 14.

Regarding H/B, its influence on N_{cse} is negligible for conditions that correspond to foundation failure mode. However, for conditions in which the relative value of $c_u/\gamma B$ with respect to H/B is small, failure mode changes from foundation failure to slope failure. This is correct for small $c_u/\gamma B$ values or for significantly high H/B values. Moreover, increases in the value of β results in conditions that are more prone to slope failure. For problems which are close to slope failure mode, H/B influences the magnitude of N_{cse} as shown in Fig. 13a, Fig. 14a, and Fig. 14b. This is the underlying reason why it is not possible to use bilinear functions to quantify the design charts. The value of λ_o is

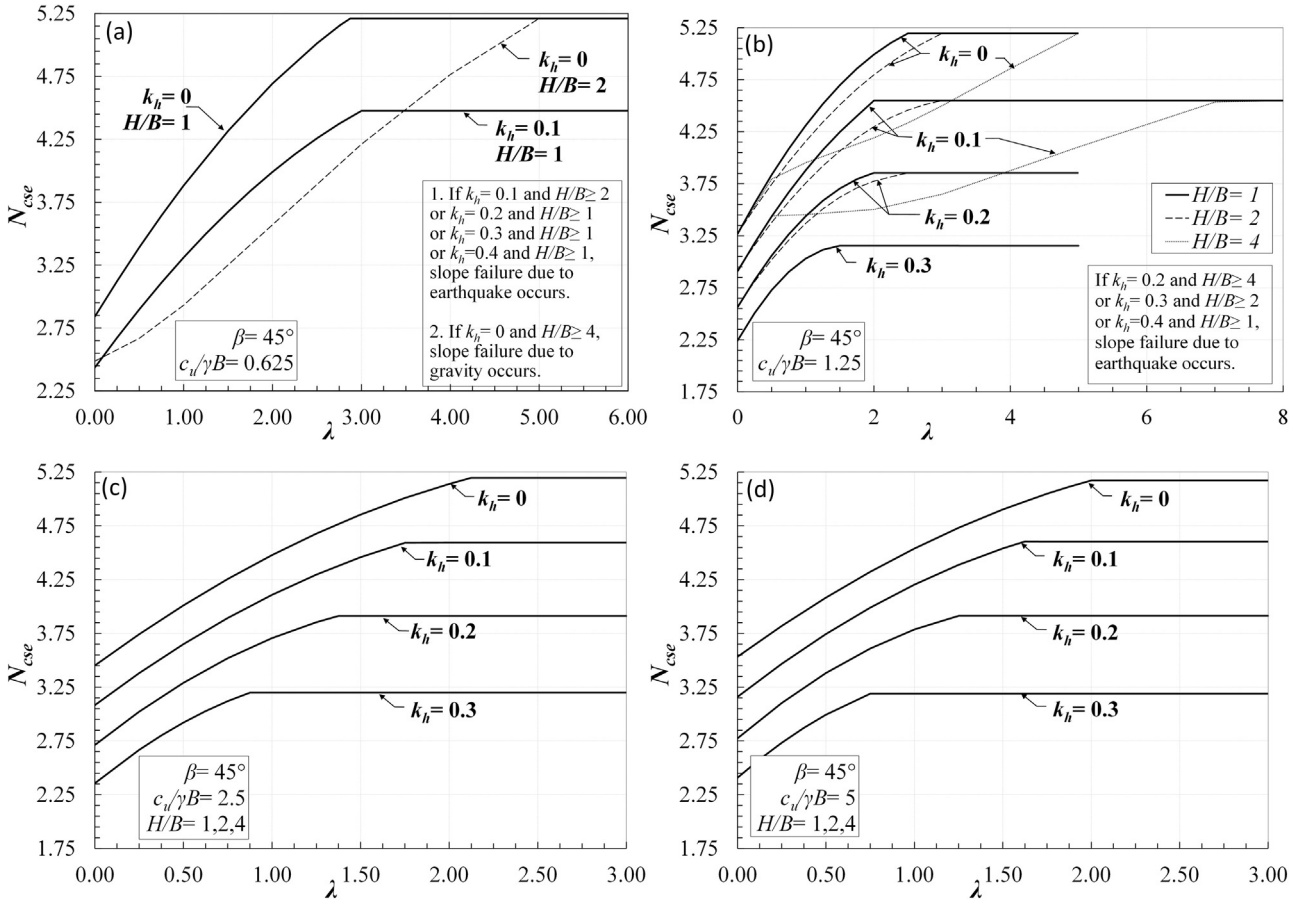

Fig. 14. Design charts for seismic bearing capacity factor of surficial strip footings located near cohesive slopes with β = 45° and H/B = 1, 2, 4 (a) $c_u/\gamma B$ = 0.625, (b) $c_u/\gamma B$ = 1.25, (c) $c_u/\gamma B$ = 2.5, (d) $c_u/\gamma B$ = 5.

dependent on the combined effects of k_h and β for conditions that clearly fail with foundation failure. However, for conditions that are close to slope failure mode, expected value of λ_o changes significantly based on the magnitude of H/B as shown in Fig. 14b. Clearly, the footing distance at which the slope influence vanishes is much greater for slopes that are closer to failure.

In the same way, $c_u/\gamma B$ affects the value of N_{cse} indirectly owing to its influence on the failure mode. As illustrated in Fig. 19, as the value of $c_u/\gamma B$ drops, corresponding values of N_{cse} reduce with an increasing rate. This is due to the fact that reduction in $c_u/\gamma B$ increases the likelihood of slope failure. That is why in Fig. 19 $c_u/\gamma B - N_{cse}$ relationships for higher k_h values lack data points for weaker soils. Missing data points correspond to conditions which failed as a slope. Slight increases in N_{cse} for high $c_u/\gamma B$ values should be ignored since this is a byproduct of the small variations between models.

Predictions of the proposed methodology yield conservative estimates of the seismic bearing capacity factor N_{cse} as a result of the inherent and explicit assumptions. First of all in the proposed study, any possible increases in strength with depth are ignored and the soil layers are assumed to constitute semi-infinite homogeneous bodies. Following the same assumption possible presence of a rigid layer underlying the slope is ignored. Pseudo-static approach is selected disregarding the variations in the ground acceleration during seismic events. Additionally, presented design charts are constructed by drawing $\lambda - N_{cse}$ relationship by remaining on the safe side. Therefore, the use of the presented design charts yield conservative estimates for N_{cse}.

8. Conclusions

Bearing capacity check is required for satisfying the stability criteria when designing shallow foundations. Even though calculation of static bearing capacity is a straightforward task for horizontal ground conditions, there is no well-defined way for considering the influences of seismicity and ground inclination. Accordingly, this parametric study proposes design charts for selecting suitable seismic bearing capacity factors for strip foundations located on or near cohesive slopes. Presented design charts are developed based on the results of numerous FEM models corresponding to different geometries, pseudo-static accelerations and undrained soil properties. Owing to the large number of influential parameters, it is not possible to quantify the results using mathematical functions. Therefore a methodology based on the selection of appropriate seismic bearing capacity factors from the proposed charts using interpolation and extrapolation is devised. Inherent and explicit assumptions used in the analysis stage and during the development of charts are all geared towards obtaining conservative estimates of the factors for calculating the ultimate seismic bearing capacity value. Obtained results were compared with similar but more limited studies available in literature for verification purposes and the results are shown.

It is observed from the results of the FEM models that there are three distinct failure modes at the ultimate state. These are sliding failure, foundation failure, and slope failure modes. Certain combinations of problem geometry, loading conditions and soil properties result in sliding failure of the foundation or slope failure of the overall system.

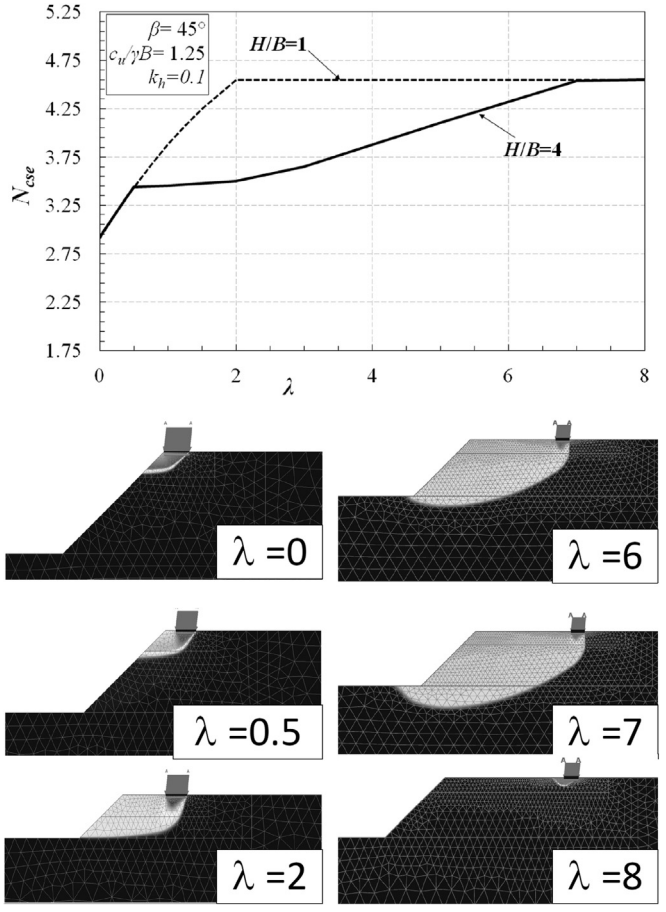

Fig. 15. Changing failure modes as λ of a foundation resting on a barely stable slope ($H/B = 4$) increases.

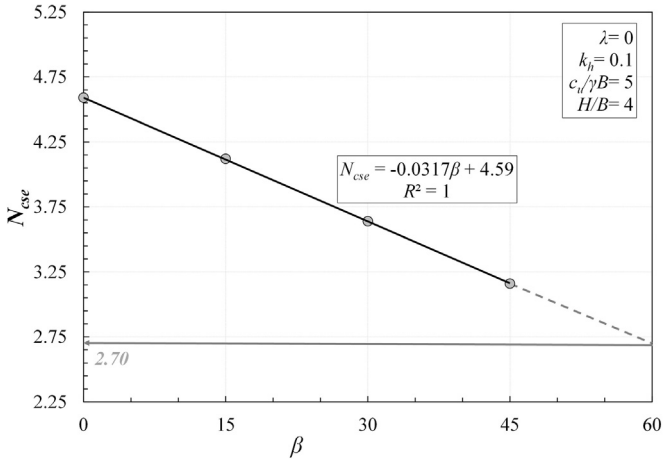

Fig. 16. Extrapolation for β = 60° (λ = 0, k_h = 0.1, $c_u/\gamma B$ = 5, H/B = 4).

Since these two conditions are intrinsically unstable, foundation bearing capacity values for these conditions are essentially zero. That is why design charts proposed in this study consider problems that fail with foundation failure mode. In case of foundation failure, resulting bearing capacity factor is shown to be a function of H/B, β, λ, $c_u/\gamma B$, and k_h. Results are presented in the form of N_{cse}–λ relationships for different combinations of k_h, $c_u/\gamma B$, and H/B. Clearly, presented N_{cse}–λ relationships have two parts. The first part of the function is relevant for foundations that are positioned close to the slope. Bearing capacity of these foundations are influenced by all five influential parameters and

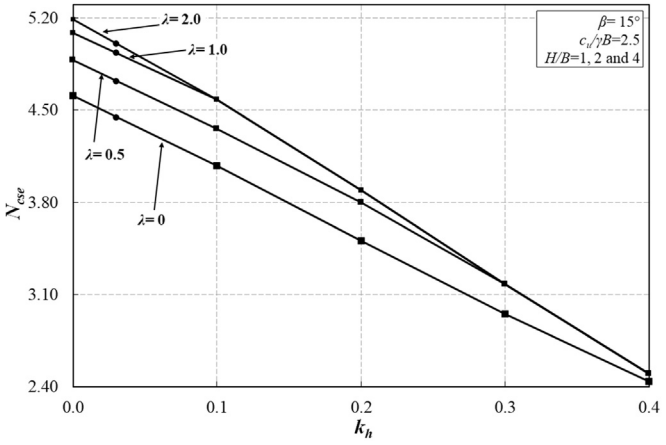

Fig. 17. Illustration of the influence of k_h on N_{cse} (β = 15°, $c_u/\gamma B$ = 2.5).

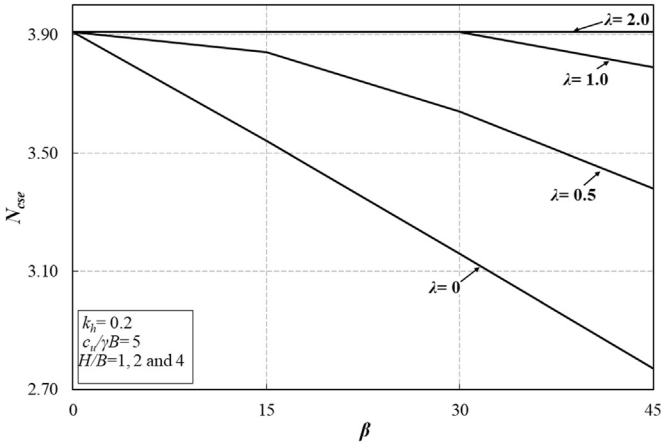

Fig. 18. Illustration of the influence of β on N_{cse} (k_h = 0.2, $c_u/\gamma B$ = 5).

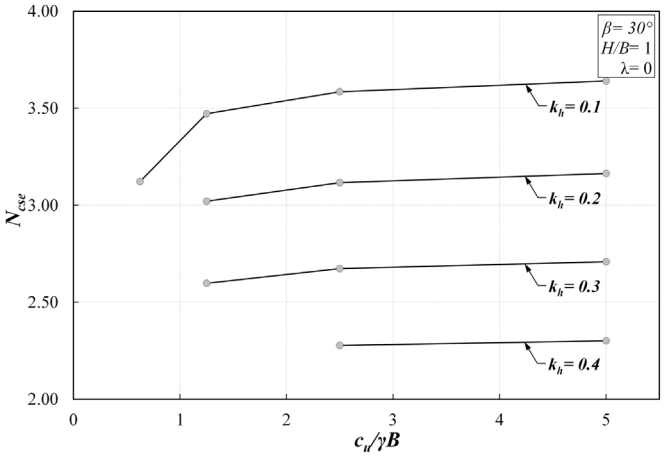

Fig. 19. Variation of N_{cse} with $c_u/\gamma B$ for all investigated k_h values (β = 30°, H/B = 1, λ = 0).

the corresponding N_{cse} increases until a limiting value. On the other hand for foundations sufficiently away from the edge of the slope, value of N_{cse} is constant at the value that is relevant for horizontal ground conditions. For this part, the value of N_{cse} is only a function of k_h as illustrated in Fig. 11. The distance at which the slope influence vanishes is λ_o. Both the value of λ_o and the mathematical form of the curve for the first part of the N_{cse}–λ relationship vary based on the proximity of the state of the problem to slope failure as exemplified in Fig. 13 and Fig. 14. For problems that are not failing as a slope but experiencing the

combined influences of relatively large k_h, β, H/B and low $c_u/\gamma B$ values, failure mode switches from bearing capacity failure to slope instability under the influence of the foundation load. For these conditions, the magnitude of λ_o is relatively higher and the rate of increase in N_{cse} with λ is smaller. Georgiadis [8] identified the same problem for static bearing capacity of footings located on or near cohesive slopes. Changes both to the form of the relationship and to its limits complicates the definition of mathematical functions with the five influential parameters. Any defined mathematical function will either be impractical or would have limited applicability. That is why this study proposed design charts for the prediction of N_{cse}. Finally, two design examples are provided demonstrating the use of the proposed design charts.

Acknowledgements

This research was supported by Bogazici University Scientific Research Project BAP12580.

References

[1] Meyerhof GG. The ultimate bearing capacity of foundation on slopes. In: Proceedings of the 4th international conference on soil mechanics: London; 1957. p. 384–386.
[2] Hansen JB. A general formula for bearing capacity. Dan Geotech Inst 1961;11:38–46.
[3] Vesic AS. Analysis of ultimate loads of shallow foundations. J Soil Mech Found Div 1973;99(SM1):45–73.
[4] Kusakabe O, Kimura T, Yamaguchi H. Bearing capacity of slopes under strip loads on the top surfaces. Soils Found 1981;21(4):29–40.
[5] Azzouz AS, Baligh MM. Loaded areas on cohesive slopes. J Geotech Eng 1983;109(5):724–9.
[6] Bowles JE. Foundation analysis and design. New York: McGraw - Hill; 1997.
[7] Castelli F, Motta E. Bearing capacity of strip footings near slopes. Geotech Geol Eng 2010;28(2):187–98.
[8] Georgiadis K. Undrained bearing capacity of strip footings on slopes. J Geotech Geoenviron Eng 2010;136(5):677–85.
[9] Georgiadis K. An upper bound solution for the undrained bearing capacity of strip footings at the top of a slope. Geotechnique 2010;60(10):801–6.
[10] Georgiadis K. The influence of load inclination on the undrained bearing capacity of strip footings on slopes. Comput Geotech 2010;37(3):311–22.
[11] Georgiadis K, Skoufaki E. Evaluation of the effective width method for strip footings on slopes under undrained loading. In: Proceedings of the 7th European conference on numerical methods in geotechnical eng. NUMGE2010: Trondheim, Norway; 2010. p. 503–507.
[12] Georgiadis K, Chrysouli E. Seismic bearing capacity of strip footings on clay slopes. In: Proceedings of the 15th European conference on soil mech. and geotechnical eng: Athens, Greece; 2011. p. 723–728.
[13] Leshchinsky B. Bearing capacity of footings placed adjacent to c′-ϕ′ slopes. J Geotech Geoenviron Eng 2015;141(6):04015022.
[14] Leshchinsky B, Xie Y. Bearing Capacity for Spread Footings Placed Near c′-ϕ′ Slopes. J Geotech Geoenviron Eng 2016;143(1):06016020.
[15] Sarma SK, Chen YC. Bearing capacity of strip footings near sloping ground during earthquakes. 11th World conference on earthquake eng.; 1996. p. 23–28.
[16] Kumar J, Rao M. Seismic bearing capacity of foundations on slopes. Geotechnique 2003;53(3):347–61.
[17] Askari F, Farzaneh O. Upper bound solution for seismic bearing capacity of shallow foundations near slopes. Geotechnique 2003;53(8):697–702.
[18] Shiau JS, Lyamin AV, Sloan SW. Application of pseudo-static limit analysis in geotechnical earthquake design. 6th European conference on numerical methods in geotech. eng.: Graz, Austria.
[19] Yamamoto K. Seismic bearing capacity of shallow foundations near slopes using the upper-bound method. Int J Geotech Eng 2010;4(2):255–67.
[20] Farzaneh O, Mofidi J, Askari F. Seismic bearing capacity of strip footings near cohesive slopes using lower bound limit analysis. In: Proceedings, 18th international conference on soil mechanics and geotechnical engineering: Paris; 2013. p. 1467–1470.
[21] Griffiths DV, Lane OA Slope stability analysis by finite elements. Geotechnique, 49(3). p. 387–403.
[22] Richards R, Shi X. Seismic lateral pressures in soils with cohesion. J Geotech Eng 1994;120(7):1230–51.
[23] Richards R, Elms DG, Budhu M. Seismic bearing capacity and settlements of foundations. J Geotech Eng 1993;119(4):662–74.
[24] Cinicioglu O, Cagbayir C. Method for the rapid evaluation of vehicle mobility on unpaved terrain. KSCE J Civ Eng 2012;16(5):742–50.
[25] Prandtl L. Uber die harte plastischer korper. Nachrichten von der Koniglichen Gesellschaft der Wissenschaften, Göttingen. Math Phys Kl 1920:74–85.
[26] Brinkgreve RBJ, Broere W, Waterman D. Plaxis User's Manual. Plaxis B. V., Delft, Netherlands; 2006.
[27] Erkli A. Seismic bearing capacity of surficial footings near cohesive slopes [M.Sc. thesis]. Istanbul, Turkey: Department of Civil Engineering, Bogazici University; 2015.
[28] Taylor DW. Stability of earth slopes. J Boston Soc Civ Eng 1937;24:197–246.
[29] Das BM, Ramana GV. Principles of soil dynamics. Stamford, USA: Cengage Learning; 2007.
[30] Koppula SD. On stability of slopes on clays with linearly increasing strength. Can Geotech J 1984;21(3):557–81.
[31] Richards R, Elms DG, Budhu M. Dynamic fluidization of soils. J Geotech Eng 1990;116(5):740–59.